



Seismic soil–structure interaction analysis of structure with shallow foundation using response spectrum method

Zhidong Gao¹ · Mi Zhao¹ · Xiuli Du¹ · Xu Zhao¹

Received: 29 August 2019 / Accepted: 19 March 2020 / Published online: 17 April 2020
© Springer Nature B.V. 2020

Abstract

Seismic soil–structure interaction (SSI) of structure with shallow foundation is studied using response spectrum method (RSM). A SSI model is first constructed with the consideration of the coupling of horizontal and rocking motions of structural foundation. In this model, the structure is modelled by finite elements and the soil by the accurate lumped parameter model (LPM) based on rational approximation. The SSI model is a non-classically damped system due to introducing damping of LPM. Complex mode superposition RSM is subsequently applied to solve the non-classically damped SSI system under design response spectrum. Seismic responses of 3-story and 6-story shear structures on two types of sites are finally calculated using the SSI model and RSM. The numerical experiments indicate that RSM can be an effective tool to analyze seismic SSI of structure with shallow foundation, and some conclusions are drawn: (1) the coupling of horizontal and rocking motions of foundation should be considered for relatively high structure on soft soil site, (2) the rational-approximation-based LPM is more accurate than the simple one, (3) the over-damped case can be neglected in the complex mode superposition process although it arises at fundamental frequency, and (4) the quasi spectrum transform relationship can be used to obtain the relative displacement and relative velocity response spectra from the given absolute acceleration design response spectrum.

Keywords Seismic soil–structure interaction · Response spectrum method · Lumped parameter model · Non-classical damping · Seismic design · Shallow foundation

1 Introduction

Soil–structure interaction (SSI) (Wolf 1986, 1988; Carbonari et al. 2011; Xiong et al. 2016; Zhao et al. 2017; Abel et al. 2018; Huang et al. 2017, 2020) significantly affects seismic responses of infrastructures, such as high-rise buildings, nuclear power plants, large-span bridges, underground structures and so on. In order to perform seismic analysis considering SSI, the suitable numerical model and method should be developed.

✉ Mi Zhao
zhaomi@bjut.edu.cn

¹ Key Laboratory of Urban Security and Disaster Engineering of Ministry of Education, Beijing University of Technology, Beijing 100124, China

Substructure model (Wolf 1994) has been widely adopted in seismic SSI analysis of aboveground structures. The model divides the whole SSI system into two substructures, i.e., a structure with rigid foundation and a massless rigid foundation–soil system. The former is modeled by finite element method so as to perform seismic analysis and design of the structure. Only the seismic SSI effects of the latter, including complex stiffness and earthquake input, require to be considered in the substructure model.

To consider the complex stiffness in time domain, the massless rigid foundation–soil system is usually modelled as a lumped parameter model (LPM) (Wolf 1986, 1994; Barros and Luco 1990; Jean et al. 1990; Lesgidis et al. 2015; Carbonari et al. 2018; González et al. 2019) that consists of springs, dashpots and mass elements. The LPMs can be divided into two main categories, namely the approximate models and the relatively accurate models. The latter is more complex due to the introduction of many auxiliary degrees of freedom. For relatively high structure on soft soil site, the rocking motions of structural foundation may cause significant influence on seismic response of structure. In such cases, the LPM systems have been developed to consider the coupling of horizontal and rocking motions of foundation (Wolf 1994; Wolf and Paronesso 1991; Wolf and Paronesso 1992; Du and Zhao 2010).

To consider the earthquake input, the so-called effective foundation input motion, that is the foundation response of the massless rigid foundation–soil system under earthquake action, should be first obtained and then transformed into an equivalent loading acting on the structural foundation (Wolf 1994). For the shallow surface foundation, the effective foundation input motion is equal to the free field motion (site response) on the ground surface (Wolf 1994).

The response spectrum method (RSM) (Sutharshana and Mcguire 1988; Berrah and Kausel 1992; Singh et al. 2000; Chopra 2011) has been widely incorporated into the codes for seismic analysis and design of aboveground structures in many countries (BSL 2000; Eurocode 8 2003; ICC 2003; GB 2010) due to its simplicity and efficiency. Recently, the method has also been developed for seismic SSI analysis of underground structure (Zhao et al. 2019). The LPM including dashpot elements will make the SSI model into a non-classically damped system. Based on the complex mode superposition RSM (Maldonad and Singh 1991; Der Kiureghian and Neuenhofer 1992; Yu and Zhou 2008; Wang and Der Kiureghian 2015; Liu et al. 2016; Chen et al. 2017), the non-classically damped system has been analyzed (Tongaonkar and Jangid 2003; AIJ 2004; Yu and Zhou 2007; Butt and Ishihara 2012; Raheem et al. 2014; Bhavikatti and Cholekar 2017). However, in the existing works, (1) the coupling between horizontal and rocking motions of structural foundation is lacking, (2) only the simple approximate LPM is used, (3) no over-damped case arise in complex mode superposition analysis, and (4) no design response spectrum is applied.

In this paper, the seismic SSI of structure with shallow foundation is solved by applying RSM to the substructure model, in which the coupled motions of horizontal and rocking of structural foundation are considered. An accurate rational-approximation-based LPM is used to consider the soil complex stiffness in time domain. The over-damped cases arise in complex mode superposition. The design response spectrum is applied to estimate the maximum seismic response of structure.

The resting parts of this paper are organized as follows. The structure with shallow foundation under earthquake is introduced in Sect. 2. The seismic SSI substructure model with LPMs is constructed in Sect. 3. The complex mode superposition RSM is summarized simply in Sect. 4. The numerical examples are given in Sect. 5 to indicate the effectiveness of RSM to analyze the seismic SSI of structure with shallow foundation. Conclusions follow in Sect. 6.

2 Structure with shallow foundation under earthquake

Figure 1a shows the structure with shallow foundation setting on soil subjected to a horizontal earthquake motion. The seismic motion is given at the surface of soil site without the structure and foundation, and its displacement time history is denoted by u_g .

The SSI is usually neglected to simplify the analysis. This model neglecting SSI is named as Model 1 in this paper. The Model 1 is the simple total fixity assumption. In this case, the displacement u_g is enforced on the structure foundation, and the soil is not considered. As shown in Fig. 1b, the dynamic finite element equation of structure with respect to absolute motion can be written as

$$\begin{bmatrix} \bar{\mathbf{M}}_R & \mathbf{0} \\ \mathbf{0} & \bar{\mathbf{M}}_B \end{bmatrix} \begin{Bmatrix} \ddot{\mathbf{u}}_R \\ \ddot{\mathbf{u}}_B \end{Bmatrix} + \begin{bmatrix} \bar{\mathbf{C}}_{RR} & \bar{\mathbf{C}}_{RB} \\ \bar{\mathbf{C}}_{BR} & \bar{\mathbf{C}}_{BB} \end{bmatrix} \begin{Bmatrix} \dot{\mathbf{u}}_R \\ \dot{\mathbf{u}}_B \end{Bmatrix} + \begin{bmatrix} \bar{\mathbf{K}}_{RR} & \bar{\mathbf{K}}_{RB} \\ \bar{\mathbf{K}}_{BR} & \bar{\mathbf{K}}_{BB} \end{bmatrix} \begin{Bmatrix} \mathbf{u}_R \\ \mathbf{u}_B \end{Bmatrix} = \begin{Bmatrix} \mathbf{0} \\ f_B \end{Bmatrix} \quad (1)$$

where \mathbf{u} , $\dot{\mathbf{u}}$ and $\ddot{\mathbf{u}}$ (or their scalar values) are the absolute horizontal displacement, velocity and acceleration, respectively; the subscripts R and B denote the degrees of freedom of superstructure and foundation, respectively; and \mathbf{M} , \mathbf{C} and \mathbf{K} are the lumped mass, damping and stiffness matrices, respectively, with the bar over matrices denoting the degrees of freedom of structure including superstructure and foundation; the three matrices are all symmetric; the displacement boundary condition gives $u_B = u_g$; and f_B denotes the reaction force of soil to foundation.

The dynamic equation can be written as the following equation with respect to the motion relative to foundation (Chopra 2011), as shown in Fig. 1c.

$$\bar{\mathbf{M}}_R \ddot{\tilde{\mathbf{u}}}_R + \bar{\mathbf{C}}_{RR} \dot{\tilde{\mathbf{u}}}_R + \bar{\mathbf{K}}_{RR} \tilde{\mathbf{u}}_R = -\bar{\mathbf{M}}_R \mathbf{I} \ddot{u}_g \quad (2)$$

where $\tilde{\mathbf{u}}_R = \mathbf{u}_R - \mathbf{I}u_g$ denotes the relative motion; and \mathbf{I} denotes the unit column vector here and all in this paper. The damping loading caused by seismic excitation is neglected on the right side of Eq. (2).

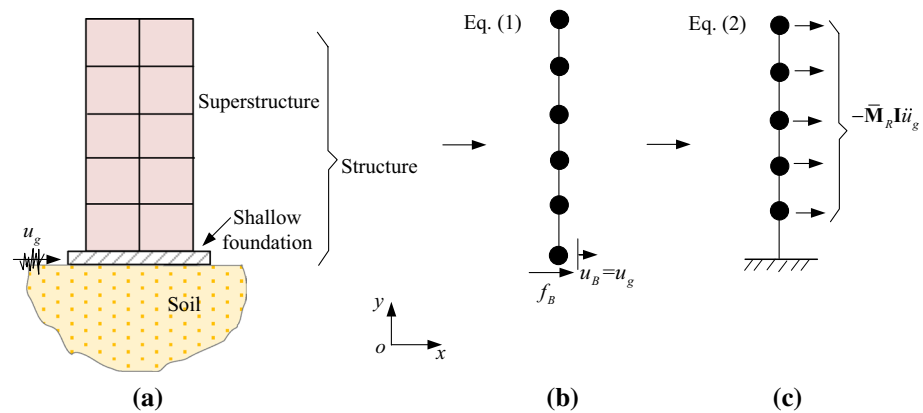


Fig. 1 Structure with shallow foundation under horizontal earthquake excitation: **a** physical problem; and seismic analysis model neglecting SSI for **b** absolute motion and **c** relative motion

3 Seismic SSI model with LPMs

Two seismic SSI models are constructed in this section. One considers only the horizontal motion of foundation, and the other considers the coupling of the horizontal and rocking motions of foundation. In the two models, the rational-approximation-based LPMs are applied to consider the soil complex stiffness in time domain more accurate relatively. Such SSI models are used in this paper to investigate the effectiveness of different SSI models.

3.1 Only horizontal motion of foundation

The seismic SSI model considering only the horizontal motion of foundation is shown in Fig. 2. It is named as Model 2 in this paper. The Model 2 accounts for foundation motion in the horizontal direction only. The physical problem is first divided and decomposed into three parts as shown in Fig. 2a. The corresponding structural model, LPM and seismic load are then presented as shown in Fig. 2b. The seismic SSI model is finally constructed with respect to the absolute and relative motions as shown in Fig. 2c.

3.1.1 Structural model

After the finite element discretization, the dynamic equation of the structure including superstructure and rigid foundation can be written as the same form as Eq. (1) with respect to the absolute motion. Here, f_B is the action force of the massless rigid foundation–soil system to the structure.

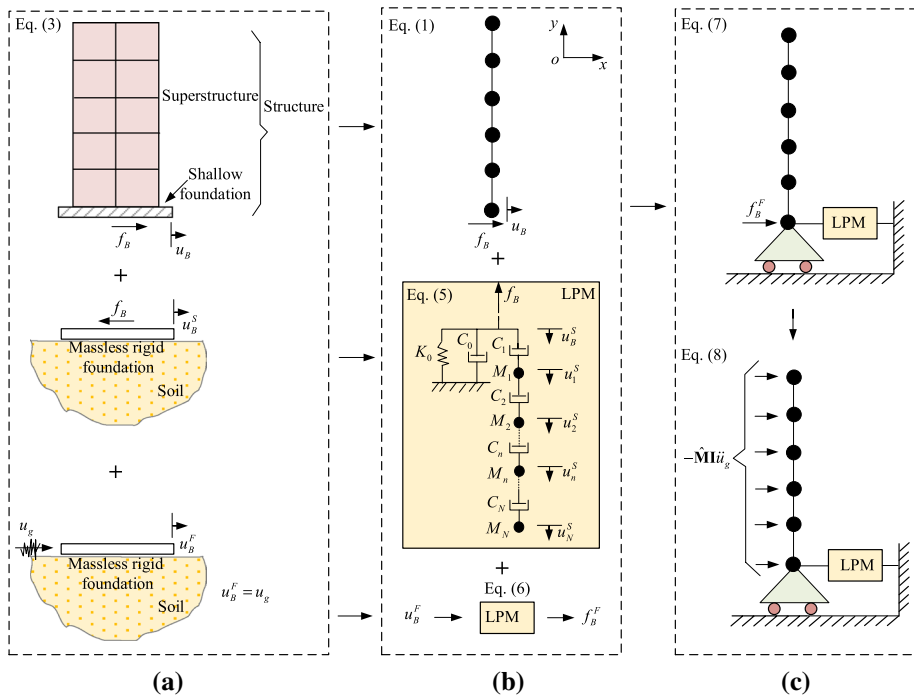


Fig. 2 Seismic SSI model considering only horizontal motion of foundation: **a** physical problem, **b** structural model, LPM and seismic load; and **c** seismic SSI model

The total absolute response in the massless rigid foundation–soil system can be decomposed into the effective foundation input motion and its relative motion on the massless rigid foundation as (Wolf 1994)

$$u_B = u_B^S + u_B^F \tag{3}$$

where u_B^F and u_B^S are the effective foundation input motion and its relative motion, respectively. For the shallow surface foundation, the effective foundation input motion is equal to the horizontal ground motion of soil site, i.e., $u_B^F = u_g$ (Wolf 1994).

3.1.2 Rational-approximation-based LPM

The complex stiffness of the massless rigid foundation–soil system can be simulated by the LPM in time domain (Wolf 1994). An accurate and stable rational-approximation-based LPM has been developed by the authors (Du and Zhao 2010) as shown in Fig. 2b.

The complex stiffness relationship between the horizontal action force f_B and horizontal relative motion u_B^S on the massless rigid foundation is first presented in frequency domain as

$$f_B(\omega) = -S_h(\omega)u_B^S(\omega) \tag{4}$$

where $S_h(\omega)$ is the horizontal stiffness of the foundation; and ω is the circular frequency with respect to time.

The horizontal stiffness is then simulated as an accurate and stable rational function of N order. The stiffness relationship Eq. (4) with the resulting rational function to replace the stiffness function is finally transformed into time domain as a LPM. The dynamic equation of LPM can be written as

$$\begin{bmatrix} 0 & \mathbf{0} \\ \mathbf{0} & \mathbf{M}_A \end{bmatrix} \begin{Bmatrix} \ddot{\mathbf{u}}_B^S \\ \ddot{\mathbf{u}}_A^S \end{Bmatrix} + \begin{bmatrix} C_{BB} & C_{BA} \\ C_{AB} & C_{AA} \end{bmatrix} \begin{Bmatrix} \dot{\mathbf{u}}_B^S \\ \dot{\mathbf{u}}_A^S \end{Bmatrix} + \begin{bmatrix} K_B & \mathbf{0} \\ \mathbf{0} & \mathbf{0} \end{bmatrix} \begin{Bmatrix} u_B^S \\ \mathbf{u}_A^S \end{Bmatrix} = \begin{Bmatrix} -f_B \\ \mathbf{0} \end{Bmatrix} \tag{5}$$

with the motion vector of the auxiliary degrees of freedom due to the relative motion

$$\mathbf{u}_A^S = \{u_1^S \ u_2^S \ \dots \ u_N^S\}^T$$

and the spring, dashpot and mass matrices

$$K_B = K_0, \ C_{BB} = C_0 + C_1, \ C_{BA} = C_{AB}^T = \{-C_1 \ 0 \ 0 \ \dots \ 0\},$$

$$C_{AA} = \begin{bmatrix} C_1 + C_2 & -C_2 & 0 & \dots & 0 & 0 \\ -C_2 & C_2 + C_3 & -C_3 & \dots & 0 & 0 \\ 0 & -C_3 & C_3 + C_4 & \dots & 0 & 0 \\ \vdots & \vdots & \vdots & \ddots & \vdots & \vdots \\ 0 & 0 & 0 & \dots & C_{N-1} + C_N & -C_N \\ 0 & 0 & 0 & \dots & -C_N & C_N \end{bmatrix} \text{ and}$$

$$M_A = \begin{bmatrix} M_1 & 0 & 0 & \dots & 0 & 0 \\ 0 & M_2 & 0 & \dots & 0 & 0 \\ 0 & 0 & M_3 & \dots & 0 & 0 \\ \vdots & \vdots & \vdots & \ddots & \vdots & \vdots \\ 0 & 0 & 0 & \dots & M_{N-1} & 0 \\ 0 & 0 & 0 & \dots & 0 & M_N \end{bmatrix}$$

where $K_0, C_n (n=0, \dots, N)$ and $M_n (n=1, \dots, N)$ are the spring, dashpot and mass element parameters; and the superscript T denotes the matrix or vector transposition.

3.1.3 Seismic load

To input earthquake on the substructure model, the effective foundation input motion $u_B^F = u_g$ is transformed into an equivalent load f_B^F acting at the structural foundation (Wolf 1994). The seismic load is equal to that applied on the LPM of Eq. (5) to cause the effective foundation input motion. It can be written as

$$\begin{bmatrix} 0 & \mathbf{0} \\ \mathbf{0} & \mathbf{M}_A \end{bmatrix} \begin{Bmatrix} \ddot{u}_B^F \\ \ddot{\mathbf{u}}_A^F \end{Bmatrix} + \begin{bmatrix} C_{BB} & C_{BA} \\ C_{AB} & C_{AA} \end{bmatrix} \begin{Bmatrix} \dot{u}_B^F \\ \dot{\mathbf{u}}_A^F \end{Bmatrix} + \begin{bmatrix} K_B & \mathbf{0} \\ \mathbf{0} & \mathbf{0} \end{bmatrix} \begin{Bmatrix} u_B^F \\ \mathbf{u}_A^F \end{Bmatrix} = \begin{Bmatrix} f_B^F \\ \mathbf{0} \end{Bmatrix} \tag{6}$$

where \mathbf{u}_A^F is the motion vector of the auxiliary degrees of freedom due to the effective foundation input motion.

3.1.4 Seismic SSI model

Adding Eqs. (6) to (5), then substituting Eq. (3) into the result, and finally assembling the result with Eq. (1), the dynamic equation of the seismic SSI model with respect to the absolute motion could be obtained as

$$\mathbf{M}\ddot{\mathbf{u}} + \mathbf{C}\dot{\mathbf{u}} + \mathbf{K}\mathbf{u} = \mathbf{F} \tag{7}$$

with

$$\begin{aligned} \mathbf{u} &= \{ \mathbf{u}_R^T \ u_B \ \mathbf{u}_A^T \}^T, \ \mathbf{u}_A = \mathbf{u}_A^S + \mathbf{u}_A^F, \ \mathbf{F} = \{ \mathbf{0} \ f_B^F \ \mathbf{0} \}^T, \\ \mathbf{M} &= \begin{bmatrix} \overline{\mathbf{M}}_R & \mathbf{0} & \mathbf{0} \\ \mathbf{0} & M_B & \mathbf{0} \\ \mathbf{0} & \mathbf{0} & \mathbf{M}_A \end{bmatrix}, \ \mathbf{K} = \begin{bmatrix} \overline{\mathbf{K}}_{RR} & \overline{\mathbf{K}}_{RB} & \mathbf{0} \\ \overline{\mathbf{K}}_{BR} & \overline{K}_{BB} + K_B & \mathbf{0} \\ \mathbf{0} & \mathbf{0} & \mathbf{0} \end{bmatrix} \text{ and} \\ \mathbf{C} &= \begin{bmatrix} \overline{\mathbf{C}}_{RR} & \overline{\mathbf{C}}_{RB} & \mathbf{0} \\ \overline{\mathbf{C}}_{BR} & \overline{C}_{BB} + C_{BB} & \mathbf{C}_{BA} \\ \mathbf{0} & \mathbf{C}_{AB} & \mathbf{C}_{AA} \end{bmatrix}. \end{aligned}$$

Transforming Eq. (7) into relative motion and neglecting the damping loading caused by seismic excitation on the right side of equation, after some manipulations, the finite element equation could be obtained as

$$\mathbf{M}\ddot{\mathbf{u}} + \mathbf{C}\dot{\mathbf{u}} + \mathbf{K}\mathbf{u} = -\hat{\mathbf{M}}\mathbf{I}\ddot{u}_g \tag{8}$$

with the relative motion and the mass matrix of inertia force

$$\tilde{\mathbf{u}} = \{ \tilde{\mathbf{u}}_R^T \ u_B^S \ \mathbf{u}_A^{ST} \}^T, \ \tilde{\mathbf{u}}_R = \mathbf{u}_R - \mathbf{I}u_g \text{ and } \hat{\mathbf{M}} = \begin{bmatrix} \overline{\mathbf{M}}_R & \mathbf{0} & \mathbf{0} \\ \mathbf{0} & M_B & \mathbf{0} \\ \mathbf{0} & \mathbf{0} & \mathbf{0} \end{bmatrix}.$$

3.2 Coupled horizontal and rocking motions of foundation

The seismic SSI model considering the coupled horizontal and rocking motions of structural foundation is shown in Fig. 3. It is named as Model 3 in this paper. The Model 3 incorporates the foundation rotation motion in a coupled manner compared with Model 2. The model is first decomposed into three parts as shown in Fig. 3a. The corresponding structural model, LPM and seismic load are then presented as shown in Fig. 3b. The seismic SSI model is finally constructed with respect to the absolute and relative motions as shown in Fig. 3c.

3.2.1 Structural model

The dynamic equation of the whole structure including the superstructure and the rigid foundation can be obtained by finite element discretization. The dynamic equation for the horizontal degrees of freedom of structure can be written similarly to the Eq. (1) as

$$\begin{bmatrix} \bar{\mathbf{M}}_R & \mathbf{0} \\ \mathbf{0} & \bar{M}_B \end{bmatrix} \begin{Bmatrix} \ddot{\mathbf{u}}_R \\ \ddot{u}_B \end{Bmatrix} + \begin{bmatrix} \bar{\mathbf{C}}_{RR} & \bar{\mathbf{C}}_{RB} \\ \bar{\mathbf{C}}_{BR} & \bar{C}_{BB} \end{bmatrix} \begin{Bmatrix} \dot{\mathbf{u}}_R - \mathbf{h}\dot{\theta}_B \\ \dot{u}_B \end{Bmatrix} + \begin{bmatrix} \bar{\mathbf{K}}_{RR} & \bar{\mathbf{K}}_{RB} \\ \bar{\mathbf{K}}_{BR} & \bar{K}_{BB} \end{bmatrix} \begin{Bmatrix} \mathbf{u}_R - \mathbf{h}\theta_B \\ u_B \end{Bmatrix} = \begin{Bmatrix} \mathbf{0} \\ f_B \end{Bmatrix} \tag{9a}$$

and the dynamic equation for the structural rotation satisfies the equilibrium equation as

$$\mathbf{h}^T \bar{\mathbf{M}}_R \ddot{\mathbf{u}}_R + \bar{J}_B \ddot{\theta}_B = Q_B \tag{9b}$$

where \mathbf{u}_R and u_B denote the total absolute horizontal displacements of superstructure and rigid foundation, respectively; θ_B denotes the rotational angle (rocking displacement) of

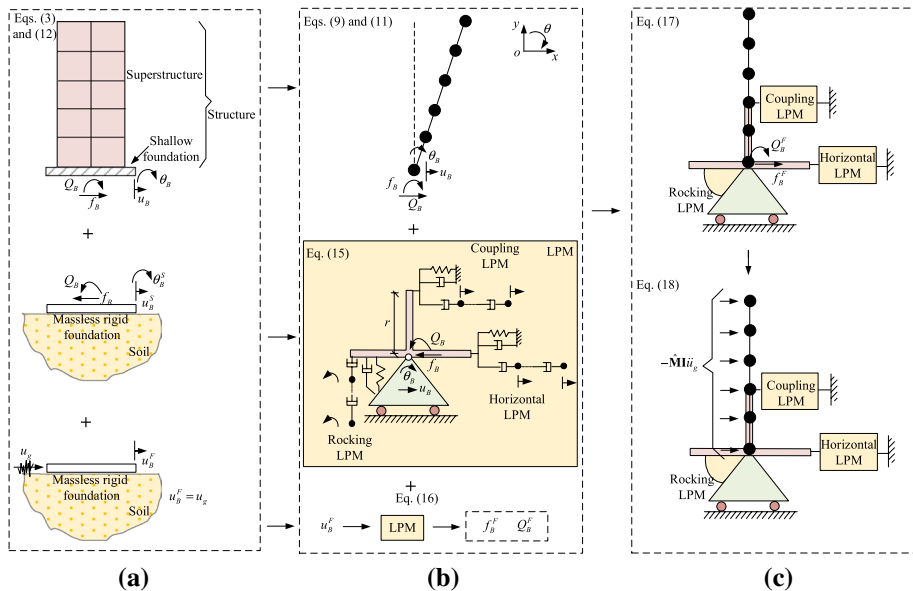


Fig. 3 Seismic SSI model considering the coupled horizontal and rocking motions of foundation: **a** physical problem, **b** structural model, LPM and seismic load; and **c** seismic SSI model

rigid foundation; $\bar{J}_B = \mathbf{h}^T \bar{\mathbf{M}}_R \mathbf{h}$ is the moment of inertia of structure; f_B and Q_B denote the action force and bending moment of the massless rigid foundation–soil system to the structure; and \mathbf{h} is a column vector of the heights of structural degrees of freedom relative to foundation.

Pre-multiplying \mathbf{h}^T to the first equation of Eq. (9a) obtains

$$\mathbf{h}^T \bar{\mathbf{M}}_R \ddot{\mathbf{u}}_R + \mathbf{h}^T \bar{\mathbf{C}}_{RR} \dot{\mathbf{u}}_R + \mathbf{h}^T \bar{\mathbf{C}}_{RB} \dot{u}_B - \mathbf{h}^T \bar{\mathbf{C}}_{RR} \mathbf{h} \dot{\theta}_B + \mathbf{h}^T \bar{\mathbf{K}}_{RR} \mathbf{u}_R + \mathbf{h}^T \bar{\mathbf{K}}_{RB} u_B - \mathbf{h}^T \bar{\mathbf{K}}_{RR} \mathbf{h} \theta_B = 0. \tag{10}$$

Combining Eqs. (10) and (9b) to eliminate the term $\mathbf{h}^T \bar{\mathbf{M}}_R \ddot{\mathbf{u}}_R$, and then assembling the result with Eq. (9a), after several manipulations, the structural dynamic equation with respect to absolute motion can be obtained as

$$\begin{aligned} & \begin{bmatrix} \bar{\mathbf{M}}_R & \mathbf{0} & 0 \\ \mathbf{0} & \bar{M}_B & 0 \\ 0 & 0 & \bar{J}_B \end{bmatrix} \begin{Bmatrix} \ddot{\mathbf{u}}_R \\ \ddot{u}_B \\ \ddot{\theta}_B \end{Bmatrix} + \begin{bmatrix} \bar{\mathbf{C}}_{RR} & \bar{\mathbf{C}}_{RB} & -\bar{\mathbf{C}}_{RR} \mathbf{h} \\ \bar{\mathbf{C}}_{BR} & \bar{C}_{BB} & -\bar{\mathbf{C}}_{BR} \mathbf{h} \\ -\mathbf{h}^T \bar{\mathbf{C}}_{RR} & -\mathbf{h}^T \bar{\mathbf{C}}_{RB} & \mathbf{h}^T \bar{\mathbf{C}}_{RR} \mathbf{h} \end{bmatrix} \begin{Bmatrix} \dot{\mathbf{u}}_R \\ \dot{u}_B \\ \dot{\theta}_B \end{Bmatrix} \\ & + \begin{bmatrix} \bar{\mathbf{K}}_{RR} & \bar{\mathbf{K}}_{RB} & -\bar{\mathbf{K}}_{RR} \mathbf{h} \\ \bar{\mathbf{K}}_{BR} & \bar{K}_{BB} & -\bar{\mathbf{K}}_{BR} \mathbf{h} \\ -\mathbf{h}^T \bar{\mathbf{K}}_{RR} & -\mathbf{h}^T \bar{\mathbf{K}}_{RB} & \mathbf{h}^T \bar{\mathbf{K}}_{RR} \mathbf{h} \end{bmatrix} \begin{Bmatrix} \mathbf{u}_R \\ u_B \\ \theta_B \end{Bmatrix} = \begin{Bmatrix} \mathbf{0} \\ f_B \\ Q_B \end{Bmatrix}. \tag{11} \end{aligned}$$

For the surface massless rigid foundation–soil system under horizontal earthquake, the effective foundation input motion is the same whether or not the foundation rotation is considered. Therefore, only the total absolute horizontal motion on the foundation is decomposed as same as Eq. (3), even though the rocking motion of foundation is considered here.

3.2.2 Rational-approximation-based LPM system

The complex stiffness of the massless rigid foundation–soil system arising from the coupled horizontal and rocking motions of the foundation can be simulated in time domain by a LPM system consisting three LPMs similar to Eq. (5), as shown in Fig. 3b.

The complex stiffness relationship between force (bending moment) and relative displacement (rotational angle) on the massless rigid foundation is first presented in frequency domain as

$$\begin{Bmatrix} f_B(\omega) \\ Q_B(\omega) \end{Bmatrix} = - \begin{bmatrix} S_h(\omega) & S_c(\omega) \\ S_c(\omega) & S_r(\omega) \end{bmatrix} \begin{Bmatrix} u_B^S(\omega) \\ \theta_B(\omega) \end{Bmatrix} = - \begin{bmatrix} S_h^m(\omega) + S_c^m(\omega) & r S_c^m(\omega) \\ r S_c^m(\omega) & S_r^m(\omega) + r^2 S_c^m(\omega) \end{bmatrix} \begin{Bmatrix} u_B^S(\omega) \\ \theta_B(\omega) \end{Bmatrix} \tag{12}$$

where $S_h(\omega)$, $S_r(\omega)$ and $S_c(\omega)$ are the horizontal, rocking and coupling stiffness functions of foundation, respectively (Wolf 1991; Wolf and Paronesso 1992; Du and Zhao 2010); $S_h^m(\omega)$, $S_r^m(\omega)$ and $S_c^m(\omega)$ are the corresponding stiffness functions of foundation which will be modelled by the three LPMs; and r denotes the half of the foundation width.

Equation (12) can be rewritten based on the modelled stiffness functions as

$$f_B(\omega) = f_{B_1}(\omega) + f_{B_2}(\omega) = -S_h^m u_B^S(\omega) - S_c^m(u_B^S(\omega) + r\theta_B(\omega)) \tag{13a}$$

$$Q_B(\omega) = r f_{B_2}(\omega) + Q_{B_3}(\omega) = -r S_c^m(\omega)(u_B^S(\omega) + r\theta_B(\omega)) - S_r^m(\omega)\theta_B(\omega) \tag{13b}$$

where the subscripts 1, 2 and 3 denote the action forces (bending moment) corresponding to the horizontal, coupling and rocking LPMs, respectively.

Three modelled stiffness functions are then simulated as three accurate and stable rational functions of N order. The three stiffness relationships with the three resulting rational functions to replace the corresponding stiffness functions are finally transformed into time domain as three LPMs similar to Eq. (5). The dynamic equations of the horizontal, coupling and rocking LPMs shown in Fig. 3b can be written respectively as

$$\begin{bmatrix} 0 & \mathbf{0} \\ \mathbf{0} & \mathbf{M}_{A_1} \end{bmatrix} \begin{Bmatrix} \ddot{u}_B^S \\ \ddot{\mathbf{u}}_{A_1}^S \end{Bmatrix} + \begin{bmatrix} C_{B_1B_1} & \mathbf{C}_{B_1A_1} \\ \mathbf{C}_{A_1B_1} & \mathbf{C}_{A_1A_1} \end{bmatrix} \begin{Bmatrix} \dot{u}_B^S \\ \dot{\mathbf{u}}_{A_1}^S \end{Bmatrix} + \begin{bmatrix} K_{B_1} & \mathbf{0} \\ \mathbf{0} & \mathbf{0} \end{bmatrix} \begin{Bmatrix} u_B^S \\ \mathbf{u}_{A_1}^S \end{Bmatrix} = \begin{Bmatrix} -f_{B_1} \\ \mathbf{0} \end{Bmatrix} \tag{14a}$$

$$\begin{bmatrix} 0 & \mathbf{0} \\ \mathbf{0} & \mathbf{M}_{A_2} \end{bmatrix} \begin{Bmatrix} \ddot{u}_R^S + r\ddot{\theta}_B \\ \ddot{\mathbf{u}}_{A_2}^S \end{Bmatrix} + \begin{bmatrix} C_{B_2B_2} & \mathbf{C}_{B_2A_2} \\ \mathbf{C}_{A_2B_2} & \mathbf{C}_{A_2A_2} \end{bmatrix} \begin{Bmatrix} \dot{u}_R^S + r\dot{\theta}_B \\ \dot{\mathbf{u}}_{A_2}^S \end{Bmatrix} + \begin{bmatrix} K_{B_2} & \mathbf{0} \\ \mathbf{0} & \mathbf{0} \end{bmatrix} \begin{Bmatrix} u_R^S + r\theta_B \\ \mathbf{u}_{A_2}^S \end{Bmatrix} = \begin{Bmatrix} -f_{B_2} \\ \mathbf{0} \end{Bmatrix} \tag{14b}$$

$$\begin{bmatrix} 0 & \mathbf{0} \\ \mathbf{0} & \mathbf{M}_{A_3} \end{bmatrix} \begin{Bmatrix} \ddot{\theta}_B \\ \ddot{\mathbf{u}}_{A_3} \end{Bmatrix} + \begin{bmatrix} C_{B_3B_3} & \mathbf{C}_{B_3A_3} \\ \mathbf{C}_{A_3B_3} & \mathbf{C}_{A_3A_3} \end{bmatrix} \begin{Bmatrix} \dot{\theta}_B \\ \dot{\mathbf{u}}_{A_3} \end{Bmatrix} + \begin{bmatrix} K_{B_3} & \mathbf{0} \\ \mathbf{0} & \mathbf{0} \end{bmatrix} \begin{Bmatrix} \theta_B \\ \mathbf{u}_{A_3} \end{Bmatrix} = \begin{Bmatrix} -Q_{B_3} \\ \mathbf{0} \end{Bmatrix}. \tag{14c}$$

3.2.3 Seismic load

As done in Sect. 3.1.3, the seismic loads, namely the applied force and bending moment are obtained by imposing the effective foundation input motion $u_B^F = u_g$ on the LPM system of Eq. (14). They can be written as

$$f_B^F = f_{B_1}^F + f_{B_2}^F \tag{15a}$$

$$Q_B^F = rf_{B_2}^F \tag{15b}$$

with

$$\begin{bmatrix} 0 & \mathbf{0} \\ \mathbf{0} & \mathbf{M}_{A_1} \end{bmatrix} \begin{Bmatrix} \ddot{u}_B^F \\ \ddot{\mathbf{u}}_{A_1}^F \end{Bmatrix} + \begin{bmatrix} C_{B_1B_1} & \mathbf{C}_{B_1A_1} \\ \mathbf{C}_{A_1B_1} & \mathbf{C}_{A_1A_1} \end{bmatrix} \begin{Bmatrix} \dot{u}_B^F \\ \dot{\mathbf{u}}_{A_1}^F \end{Bmatrix} + \begin{bmatrix} K_{B_1} & \mathbf{0} \\ \mathbf{0} & \mathbf{0} \end{bmatrix} \begin{Bmatrix} u_B^F \\ \mathbf{u}_{A_1}^F \end{Bmatrix} = \begin{Bmatrix} f_{B_1}^F \\ \mathbf{0} \end{Bmatrix} \tag{15c}$$

$$\begin{bmatrix} 0 & \mathbf{0} \\ \mathbf{0} & \mathbf{M}_{A_2} \end{bmatrix} \begin{Bmatrix} \ddot{u}_R^F \\ \ddot{\mathbf{u}}_{A_2}^F \end{Bmatrix} + \begin{bmatrix} C_{B_2B_2} & \mathbf{C}_{B_2A_2} \\ \mathbf{C}_{A_2B_2} & \mathbf{C}_{A_2A_2} \end{bmatrix} \begin{Bmatrix} \dot{u}_R^F \\ \dot{\mathbf{u}}_{A_2}^F \end{Bmatrix} + \begin{bmatrix} K_{B_2} & \mathbf{0} \\ \mathbf{0} & \mathbf{0} \end{bmatrix} \begin{Bmatrix} u_R^F \\ \mathbf{u}_{A_2}^F \end{Bmatrix} = \begin{Bmatrix} f_{B_2}^F \\ \mathbf{0} \end{Bmatrix}. \tag{15d}$$

3.2.4 Seismic SSI model

Assembling Eqs. (11), (3), (13), (14) and (15) obtains the dynamic equation of the seismic SSI model with respect to the absolute motion as

$$\mathbf{M}\ddot{\mathbf{u}} + \mathbf{C}\dot{\mathbf{u}} + \mathbf{K}\mathbf{u} = \mathbf{F} \tag{16}$$

with

$$\mathbf{u} = \left\{ \mathbf{u}_R^T \ u_B \ \theta_B \ \mathbf{u}_{A_1}^T \ \mathbf{u}_{A_2}^T \ \mathbf{u}_{A_3}^T \right\}^T, \mathbf{u}_{A_1} = \mathbf{u}_{A_1}^S + \mathbf{u}_{A_1}^F, \mathbf{u}_{A_2} = \mathbf{u}_{A_2}^S + \mathbf{u}_{A_2}^F, \mathbf{F} = \left\{ \mathbf{0} \ f_B^F \ Q_B^F \ \mathbf{0} \ \mathbf{0} \ \mathbf{0} \right\}^T,$$

$$\mathbf{M} = \begin{bmatrix} \overline{\mathbf{M}}_R & \mathbf{0} & \mathbf{0} & \mathbf{0} & \mathbf{0} & \mathbf{0} \\ \mathbf{0} & \overline{M}_B & \mathbf{0} & \mathbf{0} & \mathbf{0} & \mathbf{0} \\ \mathbf{0} & \mathbf{0} & \overline{J}_B & \mathbf{0} & \mathbf{0} & \mathbf{0} \\ \mathbf{0} & \mathbf{0} & \mathbf{0} & \mathbf{M}_{A_1} & \mathbf{0} & \mathbf{0} \\ \mathbf{0} & \mathbf{0} & \mathbf{0} & \mathbf{0} & \mathbf{M}_{A_2} & \mathbf{0} \\ \mathbf{0} & \mathbf{0} & \mathbf{0} & \mathbf{0} & \mathbf{0} & \mathbf{M}_{A_3} \end{bmatrix},$$

$$\mathbf{C} = \begin{bmatrix} \overline{\mathbf{C}}_{RR} & \overline{\mathbf{C}}_{RB} & -\overline{\mathbf{C}}_{RR}\mathbf{h} & \mathbf{0} & \mathbf{0} & \mathbf{0} \\ \overline{\mathbf{C}}_{BR} & \overline{\mathbf{C}}_{BB} + C_{B_1B_1} + C_{B_2B_2} & -\overline{\mathbf{C}}_{BR}\mathbf{h} + rC_{B_2B_2} & C_{B_1A_1} & C_{B_2A_2} & \mathbf{0} \\ -\mathbf{h}^T\overline{\mathbf{C}}_{RR} & -\mathbf{h}^T\overline{\mathbf{C}}_{RB} + rC_{B_2B_2} & \mathbf{h}^T\overline{\mathbf{C}}_{RR}\mathbf{h} + r^2C_{B_2B_2} + C_{B_3B_3} & \mathbf{0} & rC_{B_2A_2} & C_{B_3A_3} \\ \mathbf{0} & C_{A_1B_1} & \mathbf{0} & C_{A_1A_1} & \mathbf{0} & \mathbf{0} \\ \mathbf{0} & C_{A_2B_2} & rC_{A_2B_2} & \mathbf{0} & C_{A_2A_2} & \mathbf{0} \\ \mathbf{0} & \mathbf{0} & C_{A_3B_3} & \mathbf{0} & \mathbf{0} & C_{A_3A_3} \end{bmatrix},$$

$$\text{and } \mathbf{K} = \begin{bmatrix} \overline{\mathbf{K}}_{RR} & \overline{\mathbf{K}}_{RB} & -\overline{\mathbf{K}}_{RR}\mathbf{h} & \mathbf{0} & \mathbf{0} & \mathbf{0} \\ \overline{\mathbf{K}}_{BR} & \overline{\mathbf{K}}_{BB} + K_{B_1} + K_{B_2} & -\overline{\mathbf{K}}_{BR}\mathbf{h} + rK_{B_2} & \mathbf{0} & \mathbf{0} & \mathbf{0} \\ -\mathbf{h}^T\overline{\mathbf{K}}_{RR} & -\mathbf{h}^T\overline{\mathbf{K}}_{RB} + rK_{B_2} & \mathbf{h}^T\overline{\mathbf{K}}_{RR}\mathbf{h} + r^2K_{B_2} + K_{B_3} & \mathbf{0} & \mathbf{0} & \mathbf{0} \\ \mathbf{0} & \mathbf{0} & \mathbf{0} & \mathbf{0} & \mathbf{0} & \mathbf{0} \\ \mathbf{0} & \mathbf{0} & \mathbf{0} & \mathbf{0} & \mathbf{0} & \mathbf{0} \\ \mathbf{0} & \mathbf{0} & \mathbf{0} & \mathbf{0} & \mathbf{0} & \mathbf{0} \end{bmatrix}.$$

Transforming Eq. (16) into relative motion and neglecting the damping loading caused by seismic excitation on the right side of equation, after some manipulations, obtain the finite element equation as

$$\mathbf{M}\ddot{\mathbf{u}} + \mathbf{C}\dot{\mathbf{u}} + \mathbf{K}\mathbf{u} = -\hat{\mathbf{M}}\ddot{\mathbf{u}}_g \tag{17}$$

with the relative motion and the mass matrix of inertia force

$$\tilde{\mathbf{u}} = \left\{ \tilde{\mathbf{u}}_R^T \ u_B^S \ \theta_B^S \ \mathbf{u}_{A_1}^{ST} \ \mathbf{u}_{A_2}^{ST} \ \mathbf{u}_{A_3}^{ST} \right\}^T, \tilde{\mathbf{u}}_R = \mathbf{u}_R - \mathbf{I}u_g \text{ and } \hat{\mathbf{M}} = \begin{bmatrix} \overline{\mathbf{M}}_R & \mathbf{0} & \mathbf{0} & \mathbf{0} & \mathbf{0} & \mathbf{0} \\ \mathbf{0} & \overline{M}_B & \mathbf{0} & \mathbf{0} & \mathbf{0} & \mathbf{0} \\ \mathbf{0} & \mathbf{0} & \mathbf{0} & \mathbf{0} & \mathbf{0} & \mathbf{0} \\ \mathbf{0} & \mathbf{0} & \mathbf{0} & \mathbf{0} & \mathbf{0} & \mathbf{0} \\ \mathbf{0} & \mathbf{0} & \mathbf{0} & \mathbf{0} & \mathbf{0} & \mathbf{0} \\ \mathbf{0} & \mathbf{0} & \mathbf{0} & \mathbf{0} & \mathbf{0} & \mathbf{0} \end{bmatrix}$$

4 RSM for seismic SSI model

The seismic SSI model of Eqs. (8) or (17) is solved using the complex mode superposition RSM under earthquake design response spectra in this section. The complex mode analysis is first performed to consider the under- and over-damped cases (Inman and Andry 1980; Song et al. 2008; Yu and Zhou 2006). The RSM is then used with earthquake design response spectra input.

4.1 Complex mode analysis

Equations (8) or (17) is a non-classically damped system due to the consideration of SSI using the rational-approximation-based LPMs. It can be decoupled by the complex mode analysis. The details on the complex mode analysis can be seen in the references (Foss 1958; Yu and Zhou 2008). It is summarized in brief as follows.

Equations (8) or (17) can be converted into a first order matrix equation as

$$\mathbf{R}\dot{\mathbf{X}} + \mathbf{S}\mathbf{X} = -\mathbf{E}\ddot{u}_g \tag{18}$$

with

$$\mathbf{R} = \begin{bmatrix} \mathbf{0} & \mathbf{M} \\ \mathbf{M} & \mathbf{C} \end{bmatrix}, \mathbf{S} = \begin{bmatrix} -\mathbf{M} & \mathbf{0} \\ \mathbf{0} & \mathbf{K} \end{bmatrix}, \mathbf{X} = \begin{Bmatrix} \dot{\mathbf{u}} \\ \mathbf{u} \end{Bmatrix} \text{ and } \mathbf{E} = \begin{Bmatrix} \mathbf{0} \\ \hat{\mathbf{M}}\mathbf{I} \end{Bmatrix}.$$

The generalized eigenvalue problem corresponding to Eq. (18) can be written as

$$(\lambda\mathbf{R} + \mathbf{S})\Phi = \mathbf{0} \tag{19}$$

where λ and $\Phi = \{ \lambda\Phi^T \ \Phi^T \}^T$ are the generalized eigenvalue and eigenvector of Eq. (19), respectively. It can be easily proved that λ and ϕ is the complex eigenvalue and mode of Eqs. (8) or (17).

Using the above complex eigenvalues and modes, Eqs. (8) or (17) can be decoupled into the following N single-degree-of-freedom equations if the equation dimension is N .

$$\ddot{q}_j + 2\zeta_j\omega_j\dot{q}_j + \omega_j^2q_j = -\ddot{u}_g \text{ for } j = 1, 2, \dots, N \tag{20}$$

where q_j is the displacement response of the single-degree-of-freedom system; and ω_j and ζ_j are the natural frequency and damping ratio of the system, respectively.

By the superposition of the solutions of the N single-degree-of-freedom systems, the displacement response of Eqs. (8) or (17) can be written as

$$\tilde{\mathbf{u}} = \sum_{j=1}^N (\mathbf{A}_jq_j + \mathbf{B}_j\dot{q}_j) \tag{21}$$

where \mathbf{A}_j and \mathbf{B}_j are the real column vectors which are obtained from the function of modes.

4.1.1 Under-damped cases

For an under-damped equation in Eq. (20), the corresponding two eigenvalues are a pair of conjugate complex numbers. They can be written as

$$\lambda_j = -\zeta_j\omega_j + i\omega_j\sqrt{1 - \zeta_j^2} \text{ and } \hat{\lambda}_j = -\zeta_j\omega_j - i\omega_j\sqrt{1 - \zeta_j^2} \tag{22}$$

where i denotes the imaginary unit. The natural frequency and damping ratio of this under-damping equation can be obtained from Eq. (22) as

$$\omega_j = |\lambda_j| \text{ and } \zeta_j = -\frac{\text{Re}(\lambda_j)}{|\lambda_j|} \tag{23}$$

where $|\cdot|$ and $\text{Re}(\cdot)$ denote the modulus and real part of a complex number, respectively.

The two modes corresponding to the pair conjugate complex eigenvalues are also complex conjugate, and can be expressed as ϕ_j and $\hat{\phi}_j$. Using this pair of conjugate complex eigenvalues and modes and the coefficient matrices of Eqs. (8) or (17), the two vectors in Eq. (21) can be written as

$$A_j = \omega_j \zeta_j B_j - \omega_j \sqrt{1 - \zeta_j^2} \chi_j \text{ and } B_j = D_j \phi_j + \hat{D}_j \hat{\phi}_j \tag{24}$$

where

$$\chi_j = -i(D_j \phi_j - \hat{D}_j \hat{\phi}_j), D_j = \frac{-\phi_j^T \hat{M} \mathbf{I}}{2\lambda_j \phi_j^T \mathbf{M} \phi_j + \phi_j^T \mathbf{C} \phi_j} \text{ and } \hat{D}_j = \frac{-\hat{\phi}_j^T \hat{M} \mathbf{I}}{2\hat{\lambda}_j \hat{\phi}_j^T \mathbf{M} \hat{\phi}_j + \hat{\phi}_j^T \mathbf{C} \hat{\phi}_j}.$$

4.1.2 Over-damped cases

For an over-damped equation in Eq. (20), the corresponding two eigenvalues are two different real numbers. They can be written as

$$\lambda_j = -\zeta_j \omega_j + \omega_j \sqrt{\zeta_j^2 - 1} \text{ and } \hat{\lambda}_j = -\zeta_j \omega_j - \omega_j \sqrt{\zeta_j^2 - 1} \tag{25}$$

The natural frequency and damping ratio of this over-damped equation can be obtained from Eq. (25) as

$$\omega_j = \sqrt{\lambda_j \hat{\lambda}_j} \text{ and } \zeta_j = \frac{\lambda_j + \hat{\lambda}_j}{2\sqrt{\lambda_j \hat{\lambda}_j}}. \tag{26}$$

The two modes corresponding to the two real eigenvalues are also real, and can be expressed as ϕ_j and $\hat{\phi}_j$. Using the two pairs of real eigenvalues and modes and the coefficient matrices of Eqs. (8) or (17), the two vectors in Eq. (21) can be written as

$$A_j = \omega_j \zeta_j B_j - \omega_j \sqrt{\zeta_j^2 - 1} \chi_j \text{ and } B_j = D_j \phi_j + \hat{D}_j \hat{\phi}_j \tag{27}$$

where

$$\chi_j = D_j \phi_j - \hat{D}_j \hat{\phi}_j, D_j = \frac{-\phi_j^T \hat{M} \mathbf{I}}{2\lambda_j \phi_j^T \mathbf{M} \phi_j + \phi_j^T \mathbf{C} \phi_j} \text{ and } \hat{D}_j = \frac{-\hat{\phi}_j^T \hat{M} \mathbf{I}}{2\hat{\lambda}_j \hat{\phi}_j^T \mathbf{M} \hat{\phi}_j + \hat{\phi}_j^T \mathbf{C} \hat{\phi}_j}.$$

4.2 Complex mode superposition RSM

The complex complete quadratic combination (Yu and Zhou 2008; Chen et al. 2017) is adopted to combine the maximum responses of the N single-degree-of-freedom systems of Eq. (20) to obtain the maximum response of the seismic SSI system of Eqs. (8) or (17) as

$$|\tilde{u}|_{\max} = \sqrt{\sum_{j=1}^N \sum_{l=1}^N \left(\rho_{jl}^{dd} A_j A_l S_j^d S_l^d + 2\rho_{jl}^{vd} B_j A_l S_j^v S_l^d + \rho_{jl}^{vv} B_j B_l S_j^v S_l^v \right)} \tag{28}$$

where the scalar \tilde{u} , A and B denote an element of $\tilde{\mathbf{u}}$, \mathbf{A} and \mathbf{B} respectively at the same degree of freedom; $|\cdot|_{\max}$ denote the peak value of time history; $S_j^d = |q_j|_{\max}$ and $S_j^v = |\dot{q}_j|_{\max}$ are the relative displacement and relative velocity response spectra of the j th equation in Eq. (20), respectively; and ρ_{jl}^{dd} , ρ_{jl}^{vd} and ρ_{jl}^{vv} denote the displacement–displacement, displacement–velocity, velocity–displacement, and velocity–velocity cross-correlation functions between j th and l th equations in Eq. (20), respectively, and can be written as

$$\begin{aligned} \rho_{jl}^{dd} &= \frac{8\sqrt{\zeta_j \zeta_l} (g\zeta_j + \zeta_l) g^{3/2}}{(1 - g^2)^2 + 4\zeta_j \zeta_l g(1 + g^2) + 4(\zeta_j^2 + \zeta_l^2) g^2} \\ \rho_{jl}^{vd} &= \frac{4\sqrt{\zeta_j \zeta_l} (1 - g^2) g^{1/2}}{(1 - g^2)^2 + 4\zeta_j \zeta_l g(1 + g^2) + 4(\zeta_j^2 + \zeta_l^2) g^2} \\ \rho_{jl}^{vv} &= \frac{8\sqrt{\zeta_j \zeta_l} (\zeta_j + g\zeta_l) g^{3/2}}{(1 - g^2)^2 + 4\zeta_j \zeta_l g(1 + g^2) + 4(\zeta_j^2 + \zeta_l^2) g^2} \end{aligned}$$

where $g = \omega_j / \omega_l$.

The relative displacement and relative velocity response spectra with different damping ratios is required to solve Eq. (28). When using single seismic signal, the response spectra can be obtained by solving Eq. (20). When using the design response spectra, if the pseudo-acceleration response spectrum is given, the relative displacement and relative velocity response spectra can be obtained by using pseudo-spectrum transform relationship (Chopra 2011). On the other hand, the absolute acceleration design response spectrum is provided in the Chinese Code for Seismic Design of Buildings (GB 2010). It is shown in Fig. 4 with the damping ratio ζ , the characteristic period T_g , the peak ground acceleration

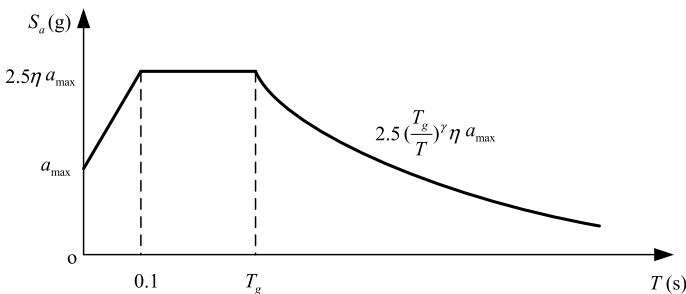


Fig. 4 Absolute acceleration design response spectrum in Chinese Code for Seismic Design of Buildings (GB 2010)

a_{\max} , and the attenuation index of descending segment and the adjustment factor of damping, respectively, as

$$\gamma = 1.0 + \frac{0.05 - \zeta}{0.3 + 6\zeta} \text{ and } \eta = 1.0 + \frac{0.05 - \zeta}{0.08 - 1.6\zeta} \tag{29}$$

From the given absolute acceleration design response spectrum S^a , the relative displacement and relative velocity design response spectra S^d and S^v can be obtained approximately by using the so-called quasi spectrum transform relationship as.

$$S^d \approx S^a / \omega^2 \tag{30-1}$$

$$S^v \approx S^a / \omega \tag{30-2}$$

where ω denotes the natural frequency of single-degree-of-freedom system.

The above method to obtain the quasi relative displacement and velocity response spectra from the absolute acceleration design one is applicable to the under-damped cases of Eq. (20). Besides, the influence of over-damped modes on computational accuracy of RSM is evaluated in Sect. 5.3. Results indicate that the over-damped mode has less influence on accuracy of RSM even if it is arise from fundamental frequency and can therefore be neglected.

5 Numerical examples

The seismic responses of a 3-story and a 6-story shear structures on two types of sites are calculated using the SSI model and RSM in this section. The problem is introduced in the first. The effects of the SSI on the seismic response of structure are then discussed using time history analysis method, including the foundation rocking effect and the different LPM effect. The RSM is finally used and its effectiveness is verified by comparing with time history analysis.

5.1 Problem statement

Figure 5 shows the 3-story and the 6-story shear structures with circular rigid foundation setting on the surface of homogeneous half-space elastic soil subjected to horizontal seismic excitation. The radius and mass of foundation are 7 m and 2.513×10^5 kg, respectively. The mass moment of inertia of the rotational rigid structure for 3-story and 6-story structures are 4.916×10^6 kg/m² and 6.858×10^6 kg/m², respectively. With axial deformations in structural elements neglected, the mass of structures is lumped at the floor level, where m_i denotes the mass at the i th floor, while k_i denotes the condensed (lateral) stiffness term at the i th floor. The mass and stiffness coefficients are given as: $m_1 = m_2 = m_3 = m_4 = m_5 = 1.036 \times 10^5$ kg, $m_6 = 8.679 \times 10^4$ kg; and $k_1 = k_2 = 9.460 \times 10^4$ kN/m, $k_3 = 9.260 \times 10^4$ kN/m, $k_4 = k_5 = 8.295 \times 10^4$ kN/m, $k_6 = 3.336 \times 10^4$ kN/m. The story heights are 3.658 m.

The damping matrix of structure complies Rayleigh rule, i.e., $\overline{\mathbf{C}}_{RR} = \alpha \overline{\mathbf{M}}_R + \beta \overline{\mathbf{K}}_{RR}$, where α and β are 1.0700 and 0.0013 respectively for 3-story structure basing on the modal damping ratio of 5%, and 0.6048 and 0.0023 for 6-story structure.

Two typical sites with homogeneous soil, namely Site 1 and Site 2, are selected to study the influence of different site conditions on structural response and calculation accuracy of

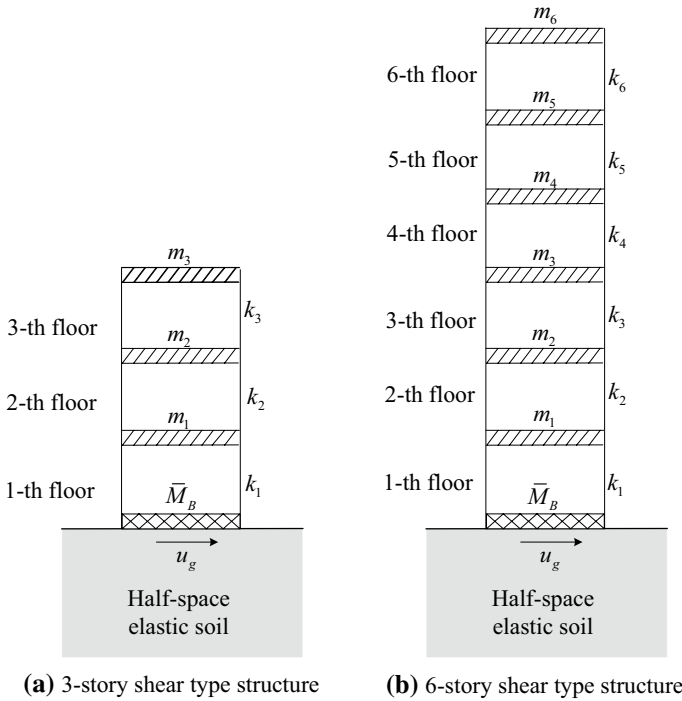


Fig. 5 Structures with shallow foundation subjected to horizontal seismic excitation

RSM. The soil density of 1560 kg/m^3 , shear wave velocity of 117 m/s , and Poisson ratio of $1/3$ are chosen for Site 1; and the soil density of 1670 kg/m^3 , shear wave velocity of 253 m/s , and Poisson ratio of $1/3$ for Site 2 are considered. The two sites belong to Class IV and II respectively according to the Chinese seismic code (GB 2010).

It is assumed that the structure is located in the region of a seismic intensity of Degree 7. The corresponding peak ground acceleration (PGA) is 0.12 g and 0.10 g for Site 1 and Site 2 respectively (i.e. probability of exceedance of 10% in 50 years) according to the Chinese seismic code (GB 2010), as shown in Table 1. Therefore, two different ground design response spectra as shown in Fig. 6 are used for the two sites. For each design spectrum, of which seven artificial ground motions are generated to be compatible with it. The response spectra of the seven artificial ground motions are also given in Fig. 6.

Table 1 Adjustment coefficient of peak ground acceleration of site

Site category	Peak ground acceleration of Class II site (g)					
	≤ 0.05	0.10	0.15	0.20	0.30	≥ 0.40
I_0	0.72	0.74	0.75	0.76	0.85	0.90
I_1	0.80	0.82	0.83	0.85	0.95	1.00
II	1.00	1.00	1.00	1.00	1.00	1.00
III	1.30	1.25	1.15	1.00	1.00	1.00
IV	1.25	1.20	1.10	1.00	0.95	0.90

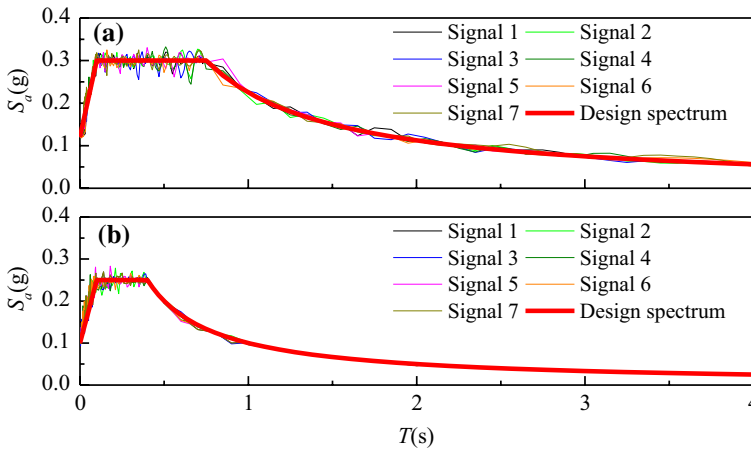


Fig. 6 Seismic acceleration response spectra with 5% damping ratio for a Site 1 and b Site 2

5.2 SSI effects on seismic response of structure

The seismic responses of the 3-story and 6-story shear structures on the two sites are calculated using time history analysis method. To study the effects of SSI on the seismic responses of structures, the Models 1, 2 and 3 mentioned above are all used for each case. In Models 2 and 3, the parameters of the rational-approximation-based LPMs are obtained according to the method in (Du and Zhao 2010) and are listed in Tables 2 and 3, respectively. To study the effects by using different LPMs on the structural responses, the simple LPM consisting parallel spring and dashpot elements is used in Model 3, too. The parameters of the simple LPM are same as K_0 and C_0 of the rational-approximation-based LPM. Signal 1 as shown in Fig. 6 is used for the time history analysis, and its acceleration time history is shown in Fig. 7. The numbers of degrees of freedom of models are presented Table 4.

Peak values of story drifts of the 3-story and 6-story structures are shown in Figs. 8 and 9, respectively. The differences between the results using Model 1, Model 2 and Model 3 with simple LPM and those using Model 3 with accurate rational-approximation-based

Table 2 Parameters of rational-approximation-based LPM for Model 2

	Site 1	Site 2
M_1	107,274	114,838
M_2	24,528	26,258
M_3	- 11,266	- 12,061
M_4	218,043	233,418
K_0	717,360,000	3,561,600,000
C_0	24,672,623	56,880,741
C_1	3,419,313	7,882,950
C_2	1,619,774	3,734,258
C_3	- 1,490,659	- 3,436,594
C_4	1,301,880	3,001,379

Table 3 Parameters of rational-approximation-based LPMs for Model 3

	Site 1				Site 2			
	Horizontal LPM	Coupled LPM	Rocking LPM	Rocking LPM	Horizontal LPM	Coupled LPM	Rocking LPM	Rocking LPM
M_1	469,045,426	20,349,713	39,748,289	39,748,289	502,119,142	21,784,629	42,551,053	42,551,053
M_2	- 289,953,166	- 105,364	407,310	407,310	- 310,398,581	- 112,794	436,031	436,031
M_3	79,112,515	380,733,957	- 8,287,336	- 8,287,336	84,690,961	407,580,582	- 8,871,699	- 8,871,699
M_4	- 124,284,947	- 285,321,008	982,040	982,040	- 133,048,629	- 305,439,797	1,051,286	1,051,286
M_5	2,601,632,758	- 192,439,675	- 2,966,287	- 2,966,287	2,785,081,222	- 206,009,139	- 3,175,448	- 3,175,448
K_0	665,279,664	57,532,272	26,695,739,392	26,695,739,392	3,303,027,840	285,640,320	132,540,907,520	132,540,907,520
C_0	- 65,018,176	- 65,018,176	- 3,429,393	- 3,429,393	- 149,894,161	- 7,906,189	- 7,906,189	- 7,906,189
C_1	93,111,761	93,111,761	691,722,271	691,722,271	214,661,652	1,594,709,892	1,594,709,892	1,594,709,892
C_2	- 117,420,861,231	- 117,420,861,231	251,510,798	251,510,798	- 270,704,322,683	579,837,855	579,837,855	579,837,855
C_3	5,799,214,095	5,799,214,095	- 231,333,394	- 231,333,394	13,369,620,246	- 533,320,476	- 533,320,476	- 533,320,476
C_4	- 10,885,055,878	- 10,885,055,878	117,016,196	117,016,196	- 25,094,618,180	269,771,399	269,771,399	269,771,399
C_5	2,825,025,590	2,825,025,590	- 156,652,199	- 156,652,199	6,512,868,589	- 361,149,007	- 361,149,007	- 361,149,007

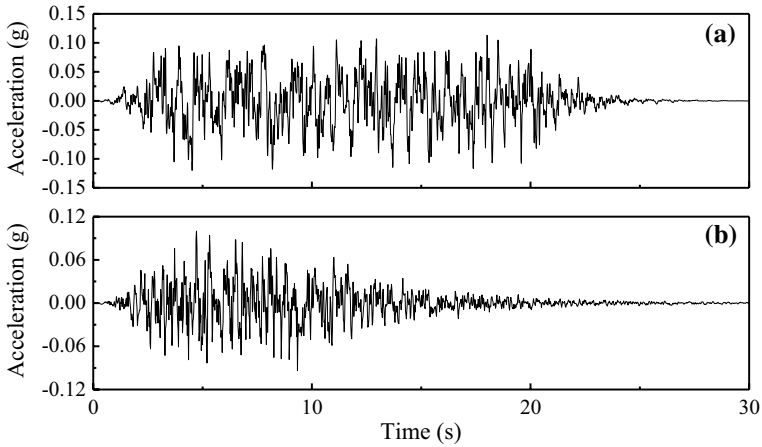


Fig. 7 Seismic acceleration time history of Signal 1 for **a** Site 1 and **b** Site 2

Table 4 Numbers of degrees of freedom of models

Model	Model 1	Model 2	Model 3 with simple LMP	Model 3 with accurate LMP
3-story structure	3	8	5	20
6-story structure	6	11	8	23

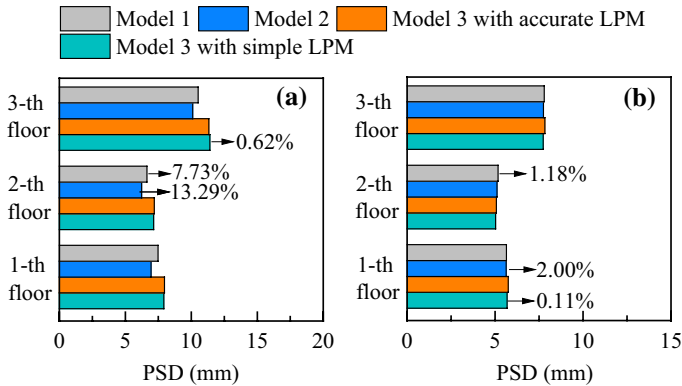


Fig. 8 Peak values of story drifts (PSD) of 3-story structure on **a** Site 1 and **b** Site 2 using four calculation models under Signal 1

LPM are calculated, and the maximum values among all floors are shown in figures. Some conclusions can be drawn for the 3-story structure from Fig. 8 as follows. For the soft soil Site 1, the SSI and rocking effects on structural responses are 7.73% and 13.29%, respectively, and the effect of different LPMs is only 0.62%. For the relatively hard soil Site 2, the effects of above factors are all less than 2%. Moreover, the Model 2 considers the SSI in the

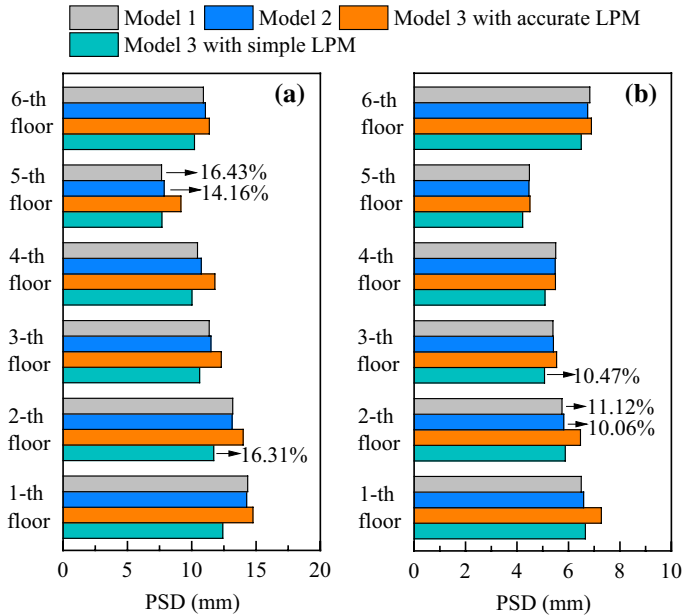


Fig. 9 Peak values of story drifts (PSD) of 6-story structure on **a** Site 1 and **b** Site 2 using four calculation models under Signal 1

horizontal direction only, and the soil radiation damping may make the structural response is less than that of Model 1. The Model 3 considers the SSI in the horizontal direction but also rotational direction, and the latter may make the structural response is more than that of Model 1. Therefore, the Model 1 may give results closer to the Model 3 than the Model 2, as shown in Fig. 8. It can be seen for the 6-story structure from Fig. 9 that the effects of above factors are from 14.16 to 16.43% for the soft soil Site 1, and from 10.06 to 11.12% for the relatively hard soil Site 2. By comparing Figs. 8 and 9, it can be seen that the rocking SSI should be considered and the accurate LPM should be used in seismic analysis of relatively high structure on soft soil site.

5.3 SSI analysis using RSM under response spectra of earthquake motions

The seismic responses of the 6-story shear structure on the two sites are calculated using RSM. The Model 3 with the accurate rational-approximation-based LPM is used to consider the coupled horizontal and rocking SSI. The result is compared with that obtained by time history analysis to evaluate the accuracy of RSM. The fourteen artificial ground motions for two sites as shown in Fig. 6 are chosen for the RSM and time history analysis.

Before using RSM to solve the SSI model, the natural frequencies and damping ratios of all single-degree-of-freedom systems of Eq. (20) are calculated by complex mode analysis in Eq. (19). When solving the generalized eigenvalue problem in Eq. (19), eight zero natural frequencies appear, due to the zero stiffness with respect to the eight auxiliary degrees of freedom in lumped parameter model. Their modes correspond to rigid body motion. Therefore, only the rest fifteen non-zero natural frequencies and corresponding damping

Table 5 Natural frequencies and damping ratios of 6-story structure on Sites 1 and 2 using Model 3 with accurate LPMs

Mode order	1	2	3	4	5	6	7	8
Structure on Site 1								
Circular frequencies (rad/s)	0.1199	6.5328	18.5195	28.0441	31.5097	39.7091	41.4599	49.4862
Damping ratios	1.9552	0.0569	0.0489	0.0530	0.7520	0.0611	0.5907	0.0667
Structure on Site 2								
Circular frequencies (rad/s)	0.2582	7.0975	18.7229	28.1280	39.7434	49.4295	56.5782	67.1105
Damping ratios	1.9552	0.0513	0.0387	0.0444	0.0548	0.0640	0.0709	0.7842
Structure on Site 1								
Natural frequencies (rad/s)	56.6036	66.0941	74.7338	80.5501	90.8454	112.7000	122.1600	
Damping ratios	0.0723	0.2904	0.2585	0.9174	0.2718	0.1325	0.1649	
Structure on Site 2								
Natural frequencies (rad/s)	77.4763	143.1780	160.6120	181.2310	195.7010	242.7180	263.0100	
Damping ratios	0.5371	0.2962	0.2589	0.9455	0.2710	0.1325	0.1641	

ratios are shown in Table 5, and the corresponding fifteen effective modes are used. It can be seen from the table that the over-damped cases arise at the fundamental frequency and some large damping ratios also arise at different natural frequencies even if they belong to the under-damped cases.

Contribution of each mode especially the over-damped mode at fundamental frequency to accuracy of RSM is studied because RSM usually uses only several main modes instead of all ones for high efficiency. The contribution ratio of each mode is quantified by defining the following relative error.

$$\bar{R} = \frac{||\bar{u}(t)||_{\max} - |u(t)|_{\max}|}{|u(t)|_{\max}} \tag{31}$$

where $|u(t)|_{\max}$ and $|\bar{u}(t)|_{\max}$ are the peak values of story drifts obtained by RSM using fifteen modes and neglecting the j th mode, respectively.

The contribution ratio of mode is calculated according to Eq. (31) and shown in Fig. 10. Dotted line in Fig. 10 denotes the level of a contribution ratio of only 1%, and the j th mode can be neglected in the subsequent analysis if the result of the Eq. (31) is below this line. Some conclusions can be drawn from Fig. 10 as follows. The over-damped mode arising at the fundamental frequency has the contribution ratio of far less than 1% of the calculation accuracy of RSM, and it can be neglected in subsequent analysis. The 2nd mode corresponding to damping ratio of about 5% has the greatest contribution ratio, and it must be included in RSM. The 3rd and 4th modes corresponding to damping ratio of near 5% have relatively great contribution, and they should be considered for high accuracy in RSM. The other modes corresponding to damping ratio from 4 to 95% have the contribution ratios of less than 1%, and they can be neglected in subsequent RSM analysis.

The structural response is calculated using RSM and time history analysis respectively under each artificial ground motions. To improve efficiency, only the 2nd–4th order modes of structure are used in RSM. The results are also compared with that obtained using the RSM with all fifteen effective modes. The corresponding natural frequencies and damping ratios for the fifteen modes are shown in Table 5. To quantify the accuracy of RSM, an error of RSM relative to time history analysis is defined as

$$R = \frac{||u(t)||_{\max} - |u_0(t)|_{\max}|}{|u_0(t)|_{\max}} \tag{32}$$

where $|u(t)|_{\max}$ and $|u_0(t)|_{\max}$ are the peak values of story drifts obtained by RSM and time history analysis, respectively.

The results are shown in Fig. 11. The error of RSM relative to time history analysis according to Eq. (32) is given for each floor in the figure, and the error of RSM using fifteen modes at the location where maximum seismic response among six floors using time analysis method is listed in red box. It can be seen that the error of RSM using fifteen modes in the red box varies from 1.45 to 4.83% for the seven ground motions of soft soil Site 1, and from 1.33 to 16.65% for the seven ground motions of relatively hard soil Site 2. The mean values of the seven ground motions are 3.55% and 7.21% for the two sites. This indicates that RSM for the SSI model is accurate enough and can be used in seismic analysis. Besides, the error of RSM result from fifteen modes and only the 2nd–4th order modes are very close. It indicates that only several main modes can be used in RSM.

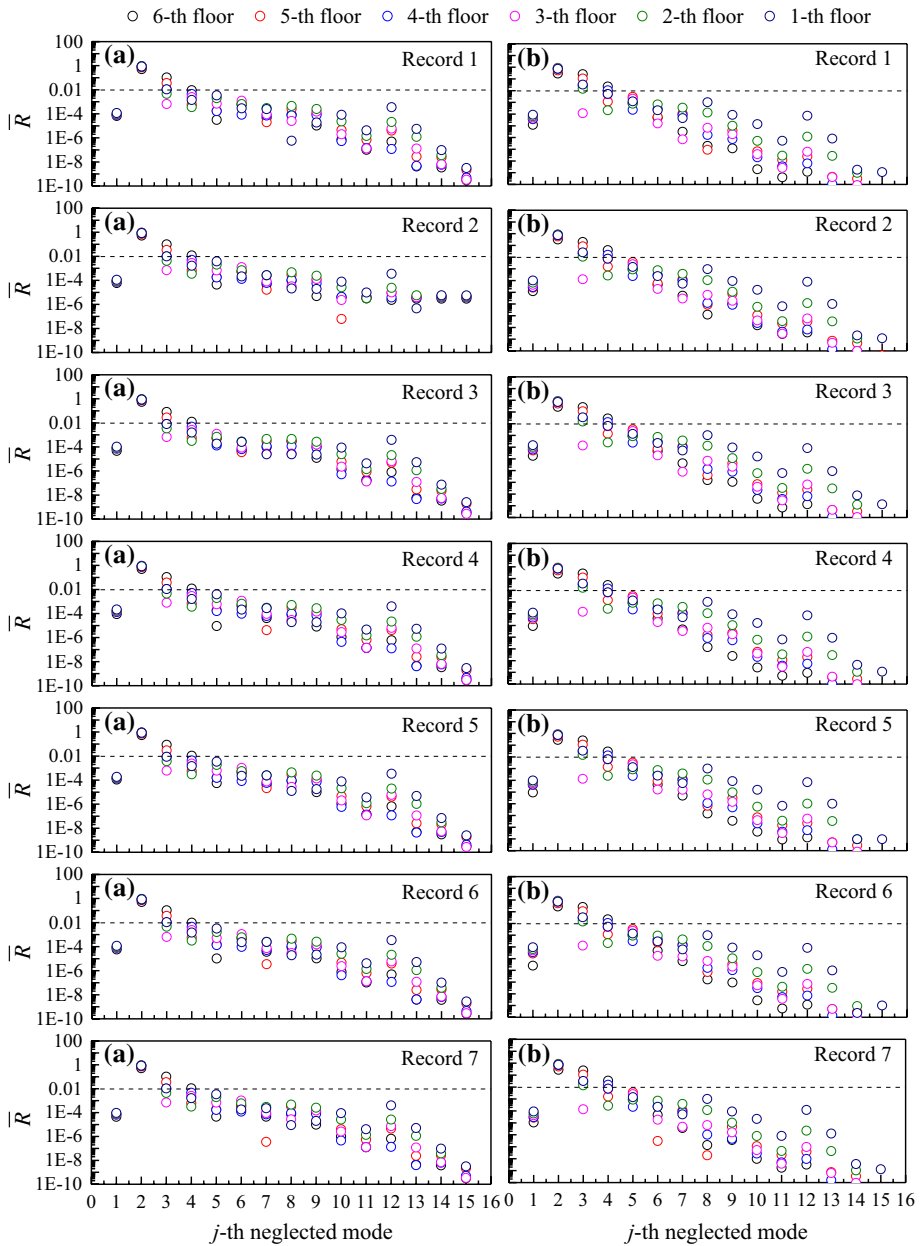


Fig. 10 Contribution ratio of j th mode on accuracy of RSM for 6-story structure on **a** Site 1 and **b** Site 2 using Model 3 with accurate LPMs under artificial ground motions

5.4 SSI analysis using RSM under design response spectra

The example and model same as Sect. 5.3 are analyzed using RSM under design response spectra shown in Fig. 6 instead of response spectra of artificial ground motions.



Fig. 11 Peak values of story drifts (PSD) of 6-story structure on **a** Site 1 and **b** Site 2 using Model 3 with accurate LPMs under artificial ground motions

The 2nd–4th order modes are used in RSM for higher efficiency. The studies in Sect. 5.3 indicate that the three modes result in very close computational results with fifteen modes. The relative displacement and relative velocity design response spectra of the 2nd–4th order modes with different damping ratios are required in RSM. They are obtained from the given absolute acceleration design response spectrum with a 5% damping ratio shown in Fig. 6 by the approximately quasi spectrum transform relationship presented in the Sect. 4.2. In order to verify the process, the so-called quasi relative displacement and velocity response spectra are compared with the mean response spectra of seven artificial ground motions obtained by solved Eq. (20), as shown in Fig. 12. In this figure, the blue circle locates at the natural frequencies shown in Table 5, which are used in calculation. It can be seen from the figure that the obtained quasi relative displacement and velocity response spectra are very close to the corresponding mean response spectra of seven artificial ground motions.

Peak values of story drifts of the 6-story structure obtained using RSM under the design response spectra and mean spectra of seven artificial ground motions are shown in Fig. 13. In addition, the mean value of peak value responses of structure obtained by time history analysis under seven artificial ground motions shown in Fig. 6 are also shown in Fig. 13 for comparison. The numbers at the side of the striped columns denote the errors in Eq. (32)

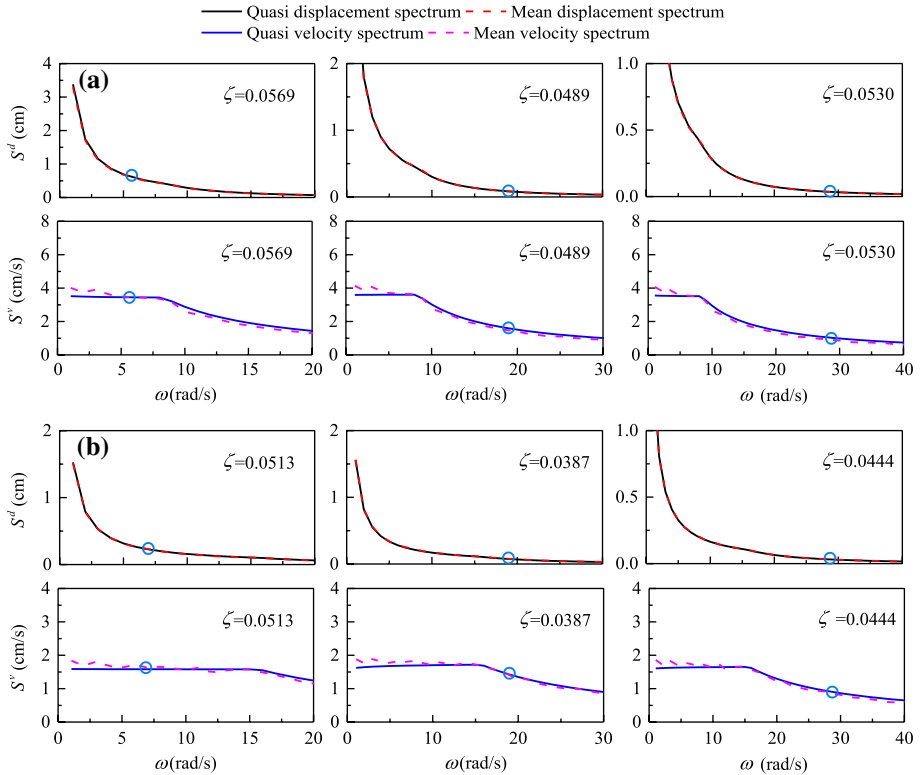


Fig. 12 Quasi spectra and mean spectra of seven ground motions for different damping ratios on **a** Site 1 and **b** Site 2

between RSM and time history analysis method, and the error at the location where maximum seismic response among six floors using time analysis method is listed in red box. The following conclusions can be drawn from the Fig. 13. The errors in the red boxes under design response spectra are close to those under mean response spectra of artificial ground motions, indicating that the method of obtaining quasi relative displacement and relative velocity response spectra is feasible. The errors in the red boxes for the Site 1 and Site 2 are less than 3% and 12% respectively, indicating that RSM is accurate enough and can be used in the seismic analysis.

6 Conclusion

Seismic SSI of structure with shallow foundation was studied using RSM. Several conclusions are drawn by analyzing the 3-story and 6-story shear structures on two different types of sites under design response spectra. (1) The coupling of the rocking motion of structural foundation with its horizontal motion should be considered for relatively high structures on soft soil site. (2) The accurate LPM such as that based on rational approximation of foundation impedance

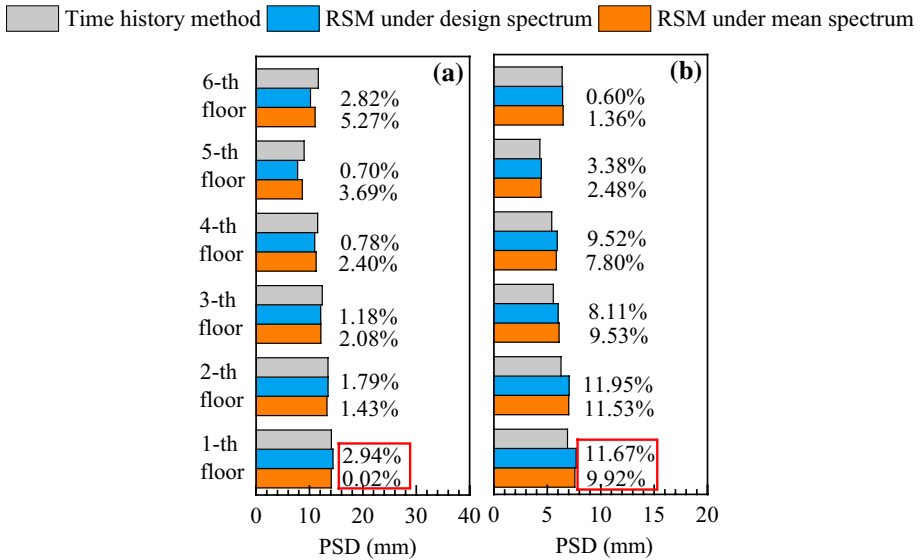


Fig. 13 Peak values of story drifts (PSD) of 6-story structure on **a** Site 1 and **b** Site 2 using Model 3 with accurate LPMs under design response spectra

function should be used in the SSI substructure model to consider the soil complex stiffness more accurate. (3) RSM is effective and applicable to seismic SSI analysis of structure with shallow foundation, where the over-damped mode can be neglected and the design response spectra can be used.

It should be noted that the above conclusions are obtained based on only the present models and examples in this paper. A complex stiffness of foundation and its time-domain model considering the hysteretic damping of site soil and deep foundation will be studied in the later work.

Acknowledgements This work described in this paper is supported by, National Basic Research Program of China (973 Program) (2015CB057902), National Key R&D Program of China (2018YFC1504305), National Natural Science Foundation of China (NSFC) (U1839201, 51678015, 51421005), Beijing Natural Science Foundation (JQ19029) and Ministry of Education Innovation Team of China (IRT_17R03). Opinions and positions expressed in this paper are those of the authors only and do not reflect those of sponsors.

References

Abel JA, Orbović N, McCallen DB, Jeremic B (2018) Earthquake soil–structure interaction of nuclear power plants, differences in response to 3-D, 3 × 1-D, and 1-D excitations. *Earthq Eng Struct Dyn* 47(6):1478–1495

AIJ (2004) Recommendations for loads on buildings. Architectural Institute of Japan, Tokyo (**in Japanese**)

Barros FCPD, Luco JE (1990) Discrete models for vertical vibrations of surface and embedded foundations. *Earthq Eng Struct Dyn* 19(2):289–303

- Berrah M, Kausel E (1992) Response spectrum analysis of structures subjected to spatially varying motions. *Earthq Eng Struct Dyn* 21(6):461–470
- Bhavikatti Q, Cholekar SB (2017) Soil structure interaction effect for a building resting on sloping ground including infill subjected to seismic analysis. *Int J Res Eng Appl Sci* 4(7):1547–1551
- BSL (2000) The building standard law of Japan. The Ministry of Construction, Tokyo (**in Japanese**)
- Butt UA, Ishihara T (2012) Seismic load evaluation of wind turbine support structures considering low structural damping and soil structure interaction. In: *European Wind Energy Association Annual Event*, Copenhagen
- Carbonari S, Morici M, Dezi F, Leoni G (2011) Seismic soil–structure interaction in multi-span bridges: application to a railway bridge. *Earthq Eng Struct Dyn* 40(11):1219–1239
- Carbonari S, Morici M, Dezi F, Leoni G (2018) A lumped parameter model for time-domain inertial soil–structure interaction analysis of structures on pile foundations. *Earthq Eng Struct Dyn* 47(11):2147–2171
- Chen HT, Tan P, Zhou FL (2017) An improved response spectrum method for non-classically damped systems. *Bull Earthq Eng* 15(10):4375–4397
- Chopra AK (2011) *Dynamics of structures: theory and applications to earthquake engineering*, 4th edn. Prentice Hall, Englewood Cliffs
- Der Kiureghian A, Neuenhofer A (1992) Response spectrum method for multi-support seismic excitations. *Earthq Eng Struct Dyn* 21(8):713–740
- Du XL, Zhao M (2010) Stability and identification for rational approximation of frequency response function of unbounded soil. *Earthq Eng Struct Dyn* 39(2):165–186
- Eurocode 8 (2003) *Design of structures for earthquake resistance*. European Committee for Standardization
- Foss FK (1958) Co-ordinates which uncouple the linear dynamic systems. *J Appl Mech ASME* 24:361–364
- GB (50011-2010) *Code for Seismic Design of Buildings China*. Architecture and Building Press, Beijing (**in Chinese**)
- González F, Padrón LA, Carbonari S, Morici M, Aznárez JJ, Dezi F, Leoni G (2019) Seismic response of bridge piers on pile groups for different soil damping models and lumped parameter representations of the foundation. *Earthq Eng Struct Dyn* 48(3):306–327
- Huang JQ, Zhao M, Du XL (2017) Non-linear seismic responses of tunnels within normal fault ground under obliquely incident P waves. *Tunn Undergr Space Technol* 61:26–39
- Huang JQ, Zhao X, Zhao M, Du XL, Wang Y, Zhang CM, Zhang CY (2020) Effect of peak ground parameters on the nonlinear seismic response of long lined tunnels. *Tunn Undergr Space Technol* 95:103175
- ICC (2003) *International building code*. International Code Council, Falls Church
- Inman DJ, Andry AN Jr (1980) Some results on the nature of eigenvalues of discrete damped linear systems. *J Appl Mech ASME* 47:927–930
- Jean WY, Tw L, Penzien J (1990) System parameters of soil foundations for time domain dynamic analysis. *Earthq Eng Struct Dyn* 19(4):541–553
- Lesgidis NL, Kwon OS, Sextos A (2015) A time-domain seismic SSI analysis method for inelastic bridge structures through the use of a frequency-dependent lumped parameter model. *Earthq Eng Struct Dyn* 44(13):2137–2156
- Liu GH, Lian JJ, Liang C, Li G, Hu JJ (2016) An improved complex multiple-support response spectrum method for the non-classically damped linear system with coupled damping. *Bull Earthq Eng* 14(1):161–184
- Maldonad GO, Singh MP (1991) An improved response spectrum method for calculating seismic design response. Part 2: Non-classically damped structures. *Earthq Eng Struct Dyn* 20(7):637–649
- Raheem SEA, Ahmed MM, Alazrek TMA (2014) Soil–structure interaction effects on seismic response of multi-story buildings on raft foundation. *J Eng Sci* 42(4):905–930
- Singh MP, Singh S, Mathew EE (2000) A response spectrum approach for seismic performance evaluation of actively controlled structures. *Earthq Eng Struct Dyn* 29(7):1029–1051
- Song J, Chu YL, Liang Z, Lee GC (2008) *Modal analysis of generally damped linear structures subjected to seismic excitations*. Technical Report. Multidisciplinary center for earthquake engineering research MCEER. SUNY at buffalo, New York
- Sutharshana S, Mcguire W (1988) Non-linear response spectrum method for three-dimensional structures. *Earthq Eng Struct Dyn* 16(6):885–900
- Tongaonkar NP, Jangid RS (2003) Seismic response of isolated bridges with soil–structure interaction. *Soil Dyn Earthq Eng* 23(4):287–302
- Wolf JP (1986) Approximate dynamic model of embedded foundation in time domain. *Earthq Eng Struct Dyn* 14(5):683–703
- Wolf JP (1988) *Soil–structure-interaction analysis in time domain*. Prentice Hall, Upper Saddle River

- Wolf JP (1994) Foundation vibrational analysis using simple physical models. Prentice Hall, Upper Saddle River
- Wolf JP, Paronesso A (1991) Errata: Consistent lumped-parameter models for unbounded soil. *Earthq Eng Struct Dyn* 20(6):597–599
- Wolf JP, Paronesso A (1992) Lumped-parameter model for a rigid cylindrical foundation embedded in a soil layer on rigid rock. *Earthq Eng Struct Dyn* 21(12):1021–1038
- Wang Z, Der Kiureghian A (2015) Multiple-support response spectrum analysis using load-dependent Ritz vectors. *Earthq Eng Struct Dyn* 43(15):2283–2297
- Xiong W, Jiang LZ, Li YZ (2016) Influence of soil–structure interaction (structure-to-soil relative stiffness and mass ratio) on the fundamental period of buildings: experimental observation and analytical verification. *Bull Earthq Eng* 14(1):139–160
- Yu RF, Zhou XY (2006) Complex mode superposition method for non-classically damped linear system with over-critical damping peculiarity. *J Build Struct* 27(1):50–59 (in Chinese)
- Yu RF, Zhou XY (2007) Simplifications of CQC method and CCQC method. *Earthq Eng Eng Vib* 6(1):65–76
- Yu RF, Zhou XY (2008) Response spectrum analysis for non-classically damped linear system with multiple-support excitations. *Bull Earthq Eng* 6(2):261–284
- Zhao M, Gao ZD, Wang LT, Du XL, Huang JQ, Li Y (2017) Obliquely incident earthquake for soil–structure interaction in layered half space. *Earthq Struct* 13(6):573–588
- Zhao M, Gao ZD, Du XL, Wang JJ, Zhong ZL (2019) Response spectrum method for seismic soil–structure interaction analysis of underground structure. *Bull Earthq Eng* 17(9):5339–5363

Publisher's Note Springer Nature remains neutral with regard to jurisdictional claims in published maps and institutional affiliations.